Journal of Materials Chemistry A

REVIEW

View Article Online
View Journal | View Issue

Cite this: *J. Mater. Chem. A*, 2021, **9**, 6013

Recent progress in aqueous zinc-ion batteries: a deep insight into zinc metal anodes

Tian Chen Li, Daliang Fang, Jintao Zhang, Mei Er Pam, Zhi Yi Leong, Juezhi Yu, Xue Liang Li, Dong Yan and Hui Ying Yang *

Received 16th September 2020
Accepted 5th January 2021

DOI: 10.1039/d0ta09111a

rsc.li/materials-a

Aqueous zinc ion batteries (AZIBs) have recently sparked an enormous surge of research attention, due to their environmental benignity, natural abundance, negligible safety issue, and exceptional electrochemical performance. Despite the rapid progress in designing a kind of exceptional cathode material with high compatibility to the aqueous electrolyte, the potential issues on the zinc anode side should not be underestimated, including dendrite growth, Zn corrosion, and hydrogen evolution. Herein, the origin of the above problems is outlined from the perspective of thermodynamics, and the optimization strategies of Zn are accordingly discussed and summarized in two aspects: the anode and the electrolyte. Finally, some general guidance and suggested future research directions for high-performance Zn anodes are proposed, aiming to further prolong cycling lifespan and promote commercialization of AZIBs.

1 Introduction

In recent years, there has been a rapid increase in demand for clean and sustainable sources of energy due to increased environmental pollution and climate change brought about by an over-reliance on fossil fuels.[1,2] Renewable energy sources derived from solar, wind or hydropower are attractive options to consider, yet their intermittent nature makes it unreliable as permanent solutions. To alleviate this problem, scientists and industrialists alike have focused their efforts on developing state-of-the-art energy storage systems to bridge the gap between supply and demand. Lithium-ion batteries (LIBs) are by far the most promising of all, yet safety issues and diminishing lithium resources make them unsustainable in the long run.[3–5] As such, there is a need to develop alternatives which are safe, inexpensive and efficient.[6–10]

Rechargeable aqueous batteries have long caught the interest of researchers due to their non-toxic nature and fast ion transfer kinetics.[11] Among the types of aqueous batteries available, zinc-ion batteries are highly prized due to their compatibility with aqueous electrolytes. Additionally, zinc metal anodes can be cheaply sourced and processed, which makes their price competitive (2.2 USD kg^{-1}) against alkali metals such as Li, Na and K.[12–14] More importantly, zinc metal possesses favorable electrochemical properties such as a relatively low redox potential of −0.76 V (*vs.* SHE), a high theoretical capacity of 820 mA h g^{-1} and an outstanding specific volumetric capacity of 5855 mA h cm^{-3}(Fig. 1a).[15]

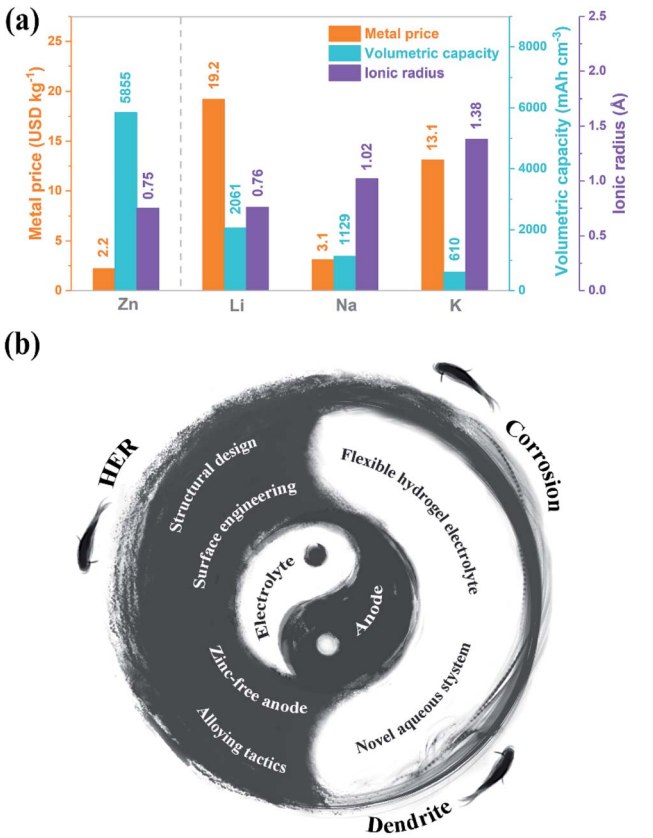

Fig. 1 (a) Comparison of metal price, volumetric capacity, and ionic radius between Zn and alkali metals. (b) Schematic illustration of the developed strategies to solve deep-seated issues of zinc metal anode for AZIBs.

Pillar of Engineering Product Development, Singapore University of Technology and Design, 8 Somapah Road, Singapore 487372, Singapore. E-mail: yanghuiying@sutd.edu.sg

In recent years, much of the work performed on aqueous zinc-ion batteries (AZIBs) was focused on developing suitable Zn^{2+} intercalation cathode hosts such as V-based oxides,[16,17] Mn-based oxides,[18] and Prussian blue analogs.[19] In comparison, there is a lack of attention given to anode materials, especially in neutral or mildly acidic electrolytes. Complementary anode materials need to be designed in order to fully realize the high energy storage capabilities of AZIBs. At present, there are three main problems plaguing zinc anodes: uncontrollable dendritic growth, corrosion and hydrogen evolution reactions (HERs).[20] Among them, rampant dendritic growth is of greatest concern. Dislocated sites within anode materials serve as thermodynamically favorable zones for Zn^{2+} nucleation to occur. Nucleation then progresses rapidly with the growth of protuberances and dendrites.[21] Although dendrite growth is suppressed to some extent with the use of acidic electrolytes,[22] rigid zinc tips possessing a high modulus still pose significant safety risks. Effects of corrosion and the HER at zinc anodes are also major bottlenecks to the commercialization of AZIBs.[23] The former is attributed to the anodic self-corrosion and electrostatic interaction between the anode surface and anions (SO_4^{2-} and OH^-) during discharge while the latter is due to the narrow electrochemical stability window of aqueous electrolytes and the formation of solvated $(Zn(H_2O)_6)^{2+}$ structure. Overall, the issues discussed in brief can occur concurrently within AZIBs and will inevitably result in the undesirable consumption of zinc metal and the electrolyte. This will lead to lowered coulombic efficiency and poor cycling performance.[13,24] To surmount these challenges, there have been many novel approaches targeted at the protection of the zinc metal anode and the stabilization of the solid–liquid interface. Therefore, a timely overview of the recent progress and comprehensive perspectives on high-performance Zn anodes are highly required, which can serve as a valuable guidance towards more efficient optimization tactics and rational material design.

In this review, we aim to provide a comprehensive discussion on the various strategies developed by researchers over the past few years and put forth our own ideas on the future of zinc anodes and AZIBs in general. We first begin by discussing the thermodynamic origins of the problems associated with zinc metal anodes and then summarize the various solutions developed to overcome these problems. These solutions include alloying, surface engineering, structural design, and adoption of zinc-free anodes, novel aqueous systems, and flexible hydrogel electrolytes (Fig. 1b). We delve deep into the fundamental mechanisms behind these strategies and discuss potential drawbacks of each. The future outlook on zinc anodes is also discussed with an emphasis on sustainable commercialization.

2 Challenges of Zn anodes

AZIBs are attracting increasingly widespread attention recently owing to their potential for large-scale energy storage with both safety and practicality. As a key component of AZIBs, Zn with many merits has been widely adopted as the anode material. The fundamental working mechanism of Zn anodes is mainly based on the Zn/Zn^{2+} electrochemical redox reaction. Therefore, reversibility in zinc plating/striping is pivotal to realize stably long cycles. However, during the development of AZIBs, researchers find that the battery performance is not as good as they expect. Based on many systematically in-depth research studies, it is recently acknowledged that zinc metal anodes in a mildly acidic electrolyte are challenged by the problems of dendrite formation and corrosion.[25,26] Furthermore, there is an added risk of H_2 evolution occurring in aqueous solution.[27] These issues are investigated in great detail and the mechanisms for failure are further discussed within this section.

2.1 Dendrite formation

A uniform distribution of electrons and ions is believed to promote smooth surface morphologies and compact metal deposits. However, the achievement of full reversibility is fundamentally hindered by the propensity of metal anodes (*e.g.*, Zn, Li, and Na) to form a non-planar surface and dendritic morphologies during metal plating.[28,29]

As acknowledged in the previous literature, lithium metal batteries exhibit the severe dendrite issue, despite having a low Young's modulus. Fortunately, the *in situ* formed solid electrolyte interphase (SEI) from decomposition products of electrolytes during cycling can protect the fresh Li surface and ensure reversible electrochemical reactions to some extent.[30] However, owing to the 1D topological and ramified structure of Li dendrites, SEIs with unfavorable mechanical strength are very likely to break and lose the defensive function, leading to unstoppable dendrite growth.[31,32] Unlike the lithium metal anode, the rampant dendrites are absent in more inactive Zn in aqueous media, and the morphology of Zn dendrites is validated to be thin hexagonal platelets (Fig. 2a). Recently, Filhol *et al.*[33] demonstrated a grand canonical DFT method to fully rationalize the dendrite morphologies associated with the growth regime of hexagonal close-packed (hcp) metals. The most stable surface of the hcp lattice is the (0001) facet, and thus the formation of the hexagonal crystal shape is preferred. As the deposition proceeds, the increased (0001) fraction results in a flattening of the particle shape as experimentally evidenced.[34] Finally, the (0001) and $(000\bar{1})$ surfaces reach the critical surface tension ($\gamma_{hkl}(E) = 0$) and force each other to increase the surface area, leading to thinner and thinner Zn platelet deposits, which is fully consistent with the experimental observation (Fig. 2b). After introducing the Zn dendrite traits, it is necessary to understand the fundamentals of Zn dendrite formation.

The dendrite formation and growth are generally triggered by inhomogeneous nucleation induced by a nonuniform Zn^{2+} concentration gradient and electric field distribution. In contrast, homogeneous nucleation has many prerequisites, such as even surface morphology, uniform interfacial electric field, and enough evenly distributed nucleation sites. However, the Zn surface is not smooth at the microscopic level. The unavoidable defects of the Zn surface during the manufacturing process serve as the nucleation seeds to form the initial protrusion, and then, zinc ions are preferentially reduced at the

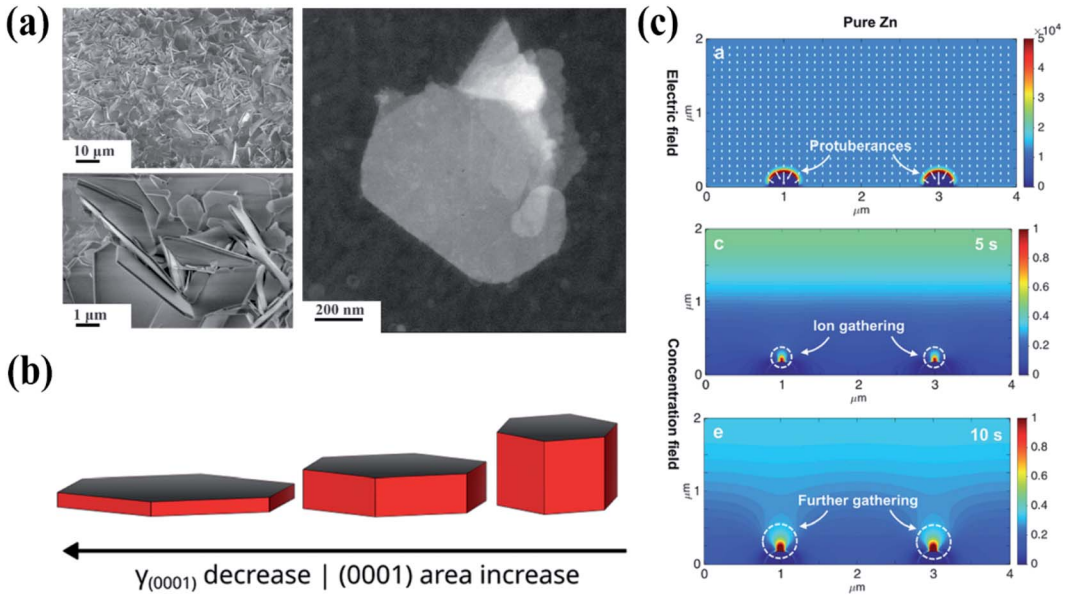

Fig. 2 (a) SEM and TEM images of Zn electrodeposits. Reproduced from ref. 38 with permission. Copyright 2019 The American Association for the Advancement of Science. (b) Schematic illustration of Zn morphology evolution during the plating process. Reproduced from ref. 39 with permission. Copyright 2020 Wiley-VCH. (c) Dual-field simulations for zinc symmetrical cells. Reproduced from ref. 33 Copyright 2020 Wiley-VCH.

irregular surface areas to minimize the surface energy. With repeated plating/striping process, the local electric field becomes more inhomogeneous and Zn^{2+} flux is concentrated on the tips, which further exacerbates the dendrite growth and capacity fading.[35,36] The initial change in the electric and concentration field is also validated by dual-field simulation (Fig. 2c). The dendrite generated during repeated cycles may drop off and become "dead zinc" or results in internal short circuit owing to its remarkably higher Young's modulus (108 GPa) than Li (5 GPa) and Na (10 GPa), particularly at high current density and depth of discharge (DOD).[37]

2.2 Corrosion and HER issues

Corrosion is a natural process that gradually deteriorates materials by chemical and/or electrochemical reaction. The refined metal can be converted into a chemically stable form when they are exposed to a specific surrounding environment. According to the Pourbaix diagram, Zn is thermodynamically active over the whole PH range.[40] In terms of AZIBs, zinc metal anodes soaked in mildly acidic $ZnSO_4$ electrolytes would generate regular hexagonal $Zn_4(OH)_6SO_4 \cdot xH_2O$ flakes (Fig. 3a).[25] The formation process can be expressed as follows:

$$Zn - 2e^- \leftrightarrow Zn^{2+} \quad (1)$$

$$4Zn^{2+} + 6OH^- + SO_4{}^{2-} + xH_2O \leftrightarrow Zn_4SO_4(OH)_6 \cdot xH_2O \quad (2)$$

The OH^- reactant is mainly originated from local PH fluctuation caused by the HER. In addition, ZnO and $Zn(OH)_2$ are also demonstrated as the by-products.[41] At present, the complicated Zn corrosion process is still elusive and worth studying further. These inert by-products loosely covering the Zn cannot effectively terminate the corrosion process because the aqueous electrolyte can penetrate through the passivated layer to react with the fresh surface. Therefore, the electrolyte and Zn are constantly consumed during cycles, leading to inferior coulombic efficiency, increased charge transfer resistance, and thus inferior battery lifespan (Fig. 3b).[26]

Another problem plaguing the zinc metal anode is the HER issue. It is uncovered that soaking zinc metals in the $ZnSO_4$ electrolyte without applied voltage would produce H_2 gas, which can be summarized by the following electrochemical reaction:[24]

$$3Zn + 11H_2O + ZnSO_4 \leftrightarrow Zn_4SO_4(OH)_6 \cdot 5H_2O + 3H_2 \quad (3)$$

In addition to this reaction, the HER is accelerated during a cathodic step (Fig. 3c). The H_2 increases the internal pressure of the air-sealed cells, and thus results in potential safety issues, such as battery swelling and even explosion (Fig. 3d).[24] Additionally, limited cyclability and electrolyte consumption are also induced by this parasitic reaction, because hydrogen reduced at the electrode surface inevitably consumes the electrons that should be provided to the Zn^{2+} charge carriers. Normally, the standard reduction potential of Zn/Zn^{2+} redox is 0.76 *vs.* the SHE, indicating the theoretically preferential reduction of H^+ from the water rather than Zn^{2+}. In fact, high kinetic overpotential exists in the process of HER for AZIBs. According to the Tafel equation, the overpotential depends on the Tafel constant, which is mainly determined by intrinsic properties of each metal.[42] Compared with other metals, Zn features a relatively high Tafel constant, resulting in effectively slower HER kinetics to some degree.[20,43] Although the situation is not as terrible as the thermodynamic model predicts, the potential

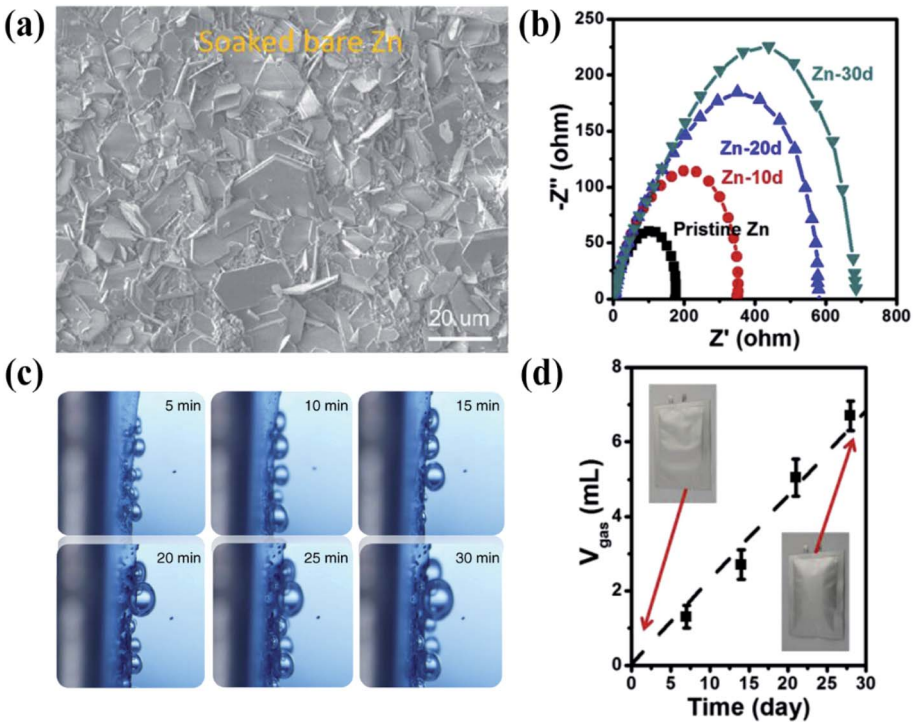

Fig. 3 (a) SEM image of bare Zn after soaking in the $ZnSO_4$ electrolyte. Reproduced from ref. 44 Copyright 2020 Wiley-VCH. (b) Increased charge transfer resistance of bare Zn after soaking in the electrolyte for one month. (c) *In situ* investigations of H_2 evolution during Zn plating in Zn/Zn cells. Reproduced from ref. 45 Copyright 2019 Nature Publishing Group. (d) Battery swelling caused by H_2 evolution. Reproduced from ref. 24 with permission. Copyright 2020 Elsevier.

risk of the HER occurring in aqueous electrolytes deserves enough attention.

3 Strategies towards high-performance Zn anodes

3.1 Anode strategies

Considerable efforts have been made to overcome the bottlenecks of uncontrolled dendrite growth and rampant side reactions in recent years. In this section, the existing solutions within the range of the anode are systematically reviewed and further categorized into four main aspects, including alloying tactics, surface engineering, structural design, and zinc-free anodes.

3.1.1 Alloying tactics. Designing zinc anodes from the perspective of alloying is simple but effective, by which the physiochemical properties can be regulated and electrochemical performances can be greatly improved.[46] Generally, an alloy is defined as metals mixed with one or more other elements. This material combines beneficial properties of two or more elements. Synergistic effects can be explored in alloys with an optimized microstructure (*i.e.*, grain size distribution and preferred grain orientation) and phase constitution (*i.e.*, solid solution, intermetallic).[47,48] To date, there are many synthetic strategies fabricating alloys. In detail, arc melting,[49,50] induction melting,[51] power metallurgy[52,53] and some coating techniques[54–56] are often applied for mass production, while in the laboratory, electrochemical alloying[24] and solution soaking[57] appear to be more flexible and facile.

Recently, two different zinc-based alloys, which are fabricated by arc melting and *in situ* electrochemical alloying respectively, have been employed as anodes for AZIBs. The former is reported by Jiang and co-workers[58] and they introduced a novel strategy named eutectic-composition alloying, which is commonly used in the field of metals and alloys and less explored in energy storage devices.[59,60] It was demonstrated that eutectic-composition alloying of zinc and aluminum as an effective strategy substantially solves the irreversibility issues of zinc anodes by making use of their lamellar structure composed of alternating zinc and aluminum nano-lamellas. More specifically, Al with a more negative reduction potential (−1.66 V *vs.* SHE) than Zn (−0.76 V *vs.* SHE) is supposed to be dissolved first. However, the natural protective mechanism endows Al lamellas with passivated alumina layers. Therefore, eliminated electrochemical activity of Al and selective zinc plating/striping are realized in the $ZnSO_4$ electrolyte. Due to the alternating Zn/Al lamellas and electrostatic field introduced by *in situ* formed alumina layers, the uncontrollable volume change and tip effects are remarkably suppressed and uniform dendrite-free deposition is achieved (Fig. 4a). Therefore, full cells constructed with the $Zn_{88}Al_{12}$ alloy anode and K_xMnO_2 cathode can deliver high-density energy (~230 W h kg^{-1}) at high levels of electrical power and retain 100% capacity after 5000 cycles (Fig. 4b).[58] Additionally, Sun *et al.*[24] demonstrated another feasible strategy, which is *in situ* electrochemical alloying

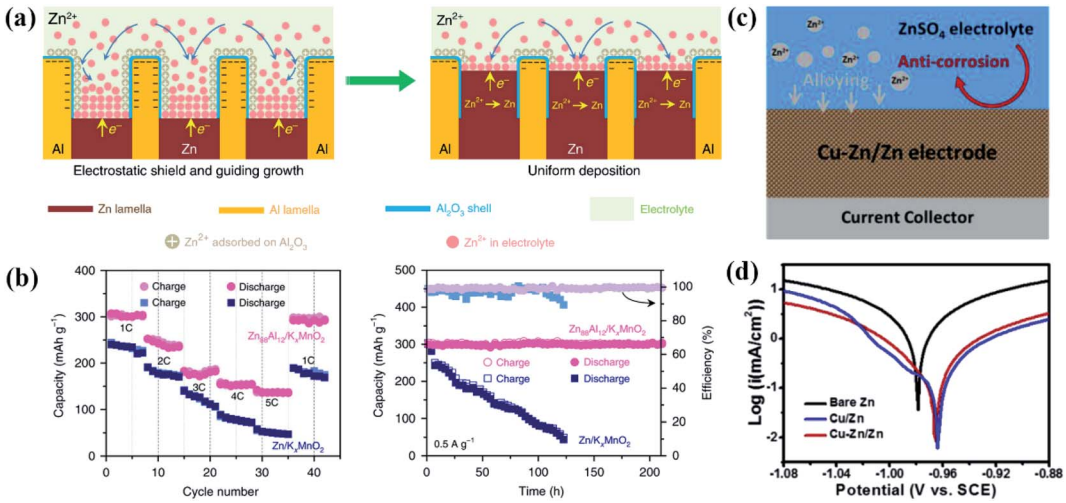

Fig. 4 (a) Schematic representation of the dendrite-suppressed mechanism regarding the Zn/Al eutectic alloy. (b) Electrochemical performance of zinc-ion full cells employing the lamellar structured Zn_{88}/Al_{12} anode. Reproduced from ref. 58 with permission. Copyright 2020 Nature Publishing Group. (c) Schematic illustration of the function of the *in situ* surface alloyed Cu–Zn/Zn electrode. (d) Linear polarization curve of three electrodes in 3 M $ZnSO_4$ electrolyte. Reproduced from ref. 24 with permission. Copyright 2020 Elsevier.

(Fig. 4c). During the cycling process, the surface of the Cu/Zn electrode is converted to the Zn–Cu/Zn alloyed interface with good electrochemical stability (Fig. 4d) and zinc affinity,[61] thus leading to superior cycling performance compared with zinc foil.

It should be pointed out that the fundamental principles of these two optimization strategies are different. The former one is achieved by nano-structural design. The typical lamellar structure is formed during the solidification because of the rationally designed eutectic composition. Such unique alternating Zn and Al lamellas can spatially redistribute the Zn^{2+} flux and facilitate homogeneous deposition within the interlayer space. Apart from Zn–Al, other eutectic systems (*i.e.* Zn–Mg and Zn–Sn) are worth further investigating.[62] For the latter research, the superior electrochemical performance is achieved by tuning the physiochemical properties to obtain exceptional corrosion resistance. Chemically stable Cu_1Zn_1 and Cu_5Zn_8 intermetallics existing on the alloy surface significantly hinder the detrimental contact with the mildly acidic environment. As a result, the corrosion reaction becomes kinetically sluggish.[63] In addition to the above alloying tactics, incorporating some elements featuring both high hydrogen evolution overpotential and good anti-corrosion capability (*i.e.* In and Pb) deserved to be considered.

3.1.2 Surface engineering. Owing to the tip effect, poor anti-corrosion resistance of Zn, and narrow stable voltage window of water, zinc plating/striping is an intrinsically unstable electrochemical behavior either in alkali or acidic aqueous solution.[20] Therefore, the surface engineering method with controllability and variability is widely adopted to reconcile the electrode/electrolyte interface, thereby facilitating uniform zinc nucleation and growth with mitigated side reactions.[64] This strategy is classified by the function of modified surface layers in this subsection: ion-coordinated layer, ion-guided layer, and electron-uniformed layer.

Some groups have recently demonstrated that the introduction of an ion-coordinated layer can provide abundant coordination sites and ion diffusion tunnels, and thus enables homogeneous ion distribution and fast charge transfer at the electrolyte/electrode interface.[35,65] For example, a novel polymer-modified zinc metal anode fabricated by doctor blading method is shown by Cui and co-workers.[66] Copious amide groups in polyamide are able to provide sufficient active sites interacting with zinc ions, leading to more stable polarization voltage than bare Zn and an ultralong lifespan of up to 8000 h. Moreover, the side reactions plaguing bare zinc during electrochemical cycles

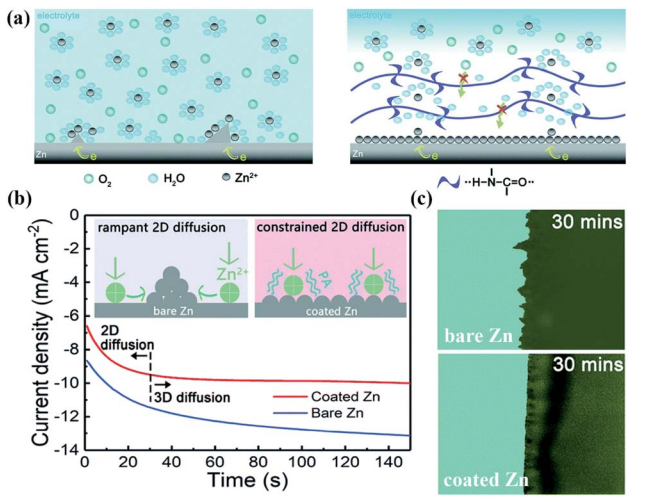

Fig. 5 (a) Schematic illustration of zinc plating on the surface of bare zinc and coated zinc, indicating the side reactions is mitigated by polyamide layer. (b) Chronoamperograms (CAs) of bare zinc and coated zinc. Insets: schematic representation of different 2D diffusion patterns. (c) The cross-sectional morphology after 30 min zinc deposition. Reproduced from ref. 66 with permission. Copyright 2019 The Royal Society of Chemistry.

are fundamentally suppressed. This is not only because the coating with water/oxygen-resistant ability serves as a buffer layer to protect the inner zinc surface but also because the solvation-sheath of zinc ions containing the detrimental H_2O molecule is destroyed by strong hydrogen bonds abundant in polyamide (Fig. 5a). Additionally, compared with bare zinc with a lasting 2D diffusion process, the diffusion mode for the coated anode evolves to initial 2D diffusion in the first 30 s, followed by a continuous and stable 3D diffusion (Fig. 5b). This means that the restricted zinc ions tend to nucleate in the vicinity of initial nucleation sites, rather than thermodynamically favorable adsorption sites with a low energy barrier. Therefore, a smooth and uniform zinc deposition pattern without dendrite growth could be observed (Fig. 5c).

Coating an ion-guided layer is another promising method to regulate the electrode/electrolyte interface. For example, Zhi *et al.* reported the *in situ* growth of hydrogen-substituted graphdiyne (HsGDY) on the zinc surface through the alkynyl-site cross-coupling reaction.[39] This coating has a semiconductor nature and sub-ångström-scale ion tunnel structure, which could serve as an ion-guided layer to spatially redistribute the Zn^{2+} concentration field and facilitate ion transportation through channels (Fig. 6a). Therefore, the lifespan of Zn@HsGDY symmetric cells is prolonged to 2400 h at 0.5 mA cm^{-2}, which is 37 times longer than that of Zn//Zn cells without protection (63 h). Pan *et al.* designed a Nafion-based ion-guided layer. They first demonstrated that the structure of solvation sheaths is modulated from six water molecules to four molecules after the introduction of the Nafion layer, indicating the decreased energy barrier, fast ion transfer kinetics and fewer side reactions. However, despite many merits of Nafion, the SO_4^{2-} and free water molecules are not completely blocked due

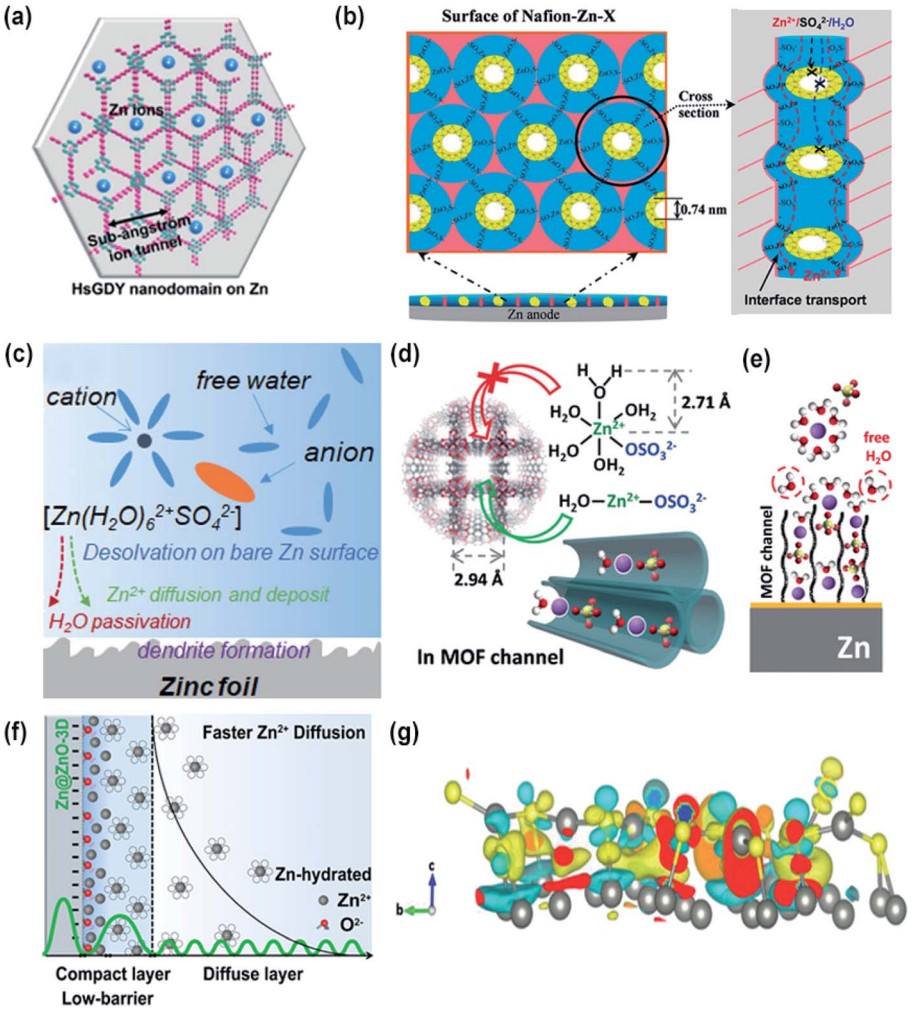

Fig. 6 (a) Sub-ångström ion channels of hydrogen-substituted graphdiyne. Reproduced from ref. 39 with permission. Copyright 2020 Wiley-VCH. (b) Ion transport mechanisms of Nafion-Zn-X protective layers. (c) Zinc foil passivated by water molecules accompanied with dendrites. Schematic illustration of (d) less hydrated ion complexes migrating through MOF channels and (e) super-saturated interface formed on the zinc surface to exclude detrimental water molecules. Reproduced from ref. 71 with permission. Copyright 2020 Wiley-VCH. (f) Schematics of the electric double layer structure and the corresponding activation energy for bare Zn and coated Zn. Reproduced from ref. 23 with permission. Copyright 2020 The Royal Society of Chemistry. (g) Electron density difference map at the interphase of ZnS@Zn. Reproduced from ref. 44 with permission. Copyright 2020 Wiley-VCH.

to the relatively large-size hydrophilic channels of Nafion. By further complexing inorganic Zn-X Zeolite nanoparticles with organic Nafion, an interfacial bridge is built *via* complexing inorganic Zn-X zeolite nanoparticles with organic Nafion. The optimized structure only allows zinc ions to hop along the hybrid interface and effectively prevent other anions and free water molecules from coming into contact with the Zn surface (Fig. 6b). In addition, some insulating materials such as Kaolin,[67] ZrO_2 (ref. 68) and $CaCO_3$ (ref. 69) are also suitable to be adopted.

Recently, the MOF materials, especially zeolitic imidazolate frameworks (ZIFs), have also attracted great attention.[70] Motivated by their molecule sieving capability, Zhou *et al.* explored the possibility of ZIF-7 modified on zinc metals. Normally, the zinc sulfate/water ion $[Zn(H_2O)_6^{2+}SO_4^{2-}]$ is desolvated on the bare zinc surface, leading to a passivated interface (Fig. 6c). By contrast, the narrow size windows of ZIF-7 (0.294 nm) endow the novel anode with the ability to exclude large-sized solvated ion complexes (Fig. 6d). Owing to the ion-guided channels, a beneficial super-saturated electrolyte is constructed on the front surface of zinc metal, forming a stable and modified electrode/electrolyte interface (Fig. 6e).[71] With the suppression of corrosion and H_2 evolution, the decorated Zn coupled with MnO_2 exhibits a high capacity retention of 88.9% after 600 cycles.

However, it is worth noting that most artificial layers are coated on the Zn surface *via* the doctor-blading method and inevitably suffered from poor bonding strength and local inhomogeneity. They are very likely to break and peel off due to the repeated volume change during cycling. Therefore, developing a robust and dense artificial SEI without significantly sacrificing ion conductivity is a good way to comprehensively solve the problems. To solve this potential issue, Zhou *et al.*[23] designed the *in situ* coated 3D nanoporous ZnO architecture on the Zn plate through $Zn(OH)_4^{2-}$ ion deposition. The novel ZnO-3D layer can accelerate the redox kinetics and increase the transference number of active species by selectively attracting Zn^{2+} rather than the hydrated complex in electric double layers (Fig. 6f). As a result, the uncontrolled dendrite growth and side reactions are simultaneously reduced. Accordingly, the full cells exhibit excellent durability over 500 cycles with a specific capacity of 212.9 mA h g^{-1}. Additionally, Guo *et al.*[44] also built an *in situ* dense ZnS artificial layer on the Zn surface *via* a facile vapor-solid strategy. The unbalanced charge distribution at the interphase, as illustrated in Fig. 6g, accelerates the Zn^{2+} flux and ensures the structure integrity. This layer not only serves as a protective barrier to mitigate the corrosion but also acts as an ion-guided layer to make the zinc deposition uniform and realize high-performance zinc anodes.

Based on the above discussion, there are some features that the ion-guided layer should have: (1) enough physical strength to withstand inner stress; (2) good corrosion resistance and electrochemical stability to keep the structural integrity; (3) electron-insulating ability and homogeneous porous surface to guide Zn^{2+}; and favorable ion tunnels to facilitate ion diffusion and reduce the desolvation energy barrier.

In addition, an electron-uniformed surface layer can also be a feasible strategy to promote the cycling stability of zinc metal anode for AZIBs. For example, carbonaceous materials with outstanding electrical conductivity have been reported as an effective electron-uniformed surface layer to stabilize the zinc metal anode. This is because zinc ions are inclined to be homogeneously distributed under a stable electric field caused by the porous carbon network.[64] Therefore, zinc metal modified with a 3D carbon-based framework, such as rGO,[72–74] CNT[75] and ZIF-8 derived carbon,[76] enables greatly improved cycling stability. Recently, Zhang *et al.*[77] engineered a functional graphite coating on the Zn surface *via* a novel pencil-drawing method. With the help of high conductivity and the capability to homogenize the electric field distribution, this artificial electron-uniformed layer can function as a porous nucleus inducer and dendrite inhibitor. However, it is worth noting that the zinc species prefers to be reduced on the interface with both electrons and ions. This further indicates that the carbonaceous modified layers have some natural drawbacks, that is, side reaction issues are still not effectively solved due to the undesirable zinc deposition on the carbon surface. Moreover, pulverization of the doctor-blading film may also take place.

3.1.3 Structural design. For alkali zinc-based batteries, structurally designed zinc metal, such as zinc-sponge[78] and monolithic nanoporous zinc,[79] is a superior choice to realize uniform deposition.[14] Even under a high DOD, the structure can be well retained. However, a larger surface area will inevitably contribute to more undesirable byproducts especially when the electrolyte is mildly acidic.[13] Hence, other alternative strategies should be considered for AZIBs.

Designing a 3D host for lithium metals has been very popular recently, in view of the serious dendrite issue.[80,81] Likewise, an inspiring tactics can be adopted in AZIBs. A conductive 3D host with higher zinc loads and lower voltage hysteresis can modify the zinc/host interface and correspondingly promote electrochemical performance for a zinc anode. A copper 3D scaffold is one of the representative 3D hosts, which not only serves as a current collector to conduct electrons but also provides a spatially homogeneous space to accommodate zinc.[82,83] In addition, some other studies also focus on carbonaceous substrates (*e.g.*, CNT paper,[84] carbon cloth (CC),[85] graphene foam,[86] and ZIF-8 derived carbon[87]). The inherently promising electrical conductivity and highly porous architecture enables homogeneous interfacial charge distribution and thus smooth surface plating. For instance, Lu *et al.*[88] reported a successful application case of a hierarchical CNT framework. More specifically, CC decorated with interconnected CNT exhibits a uniform deposition pattern due to the regulated current density (Fig. 7a) and consequently better electrochemical performance (Fig. 7b).[88] In strong contrast, an inhomogeneous electric field distribution is revealed on nucleus sites of bare CC. Such an intense charge gradient enables zinc ions to preferentially deposit on these protuberances, which ultimately causes obvious dendrite growth. Metallic substrates and carbon scaffolds have their pros and cons. The production process of metallic substrates is facile and time-saving, but their high density would significantly reduce energy density.

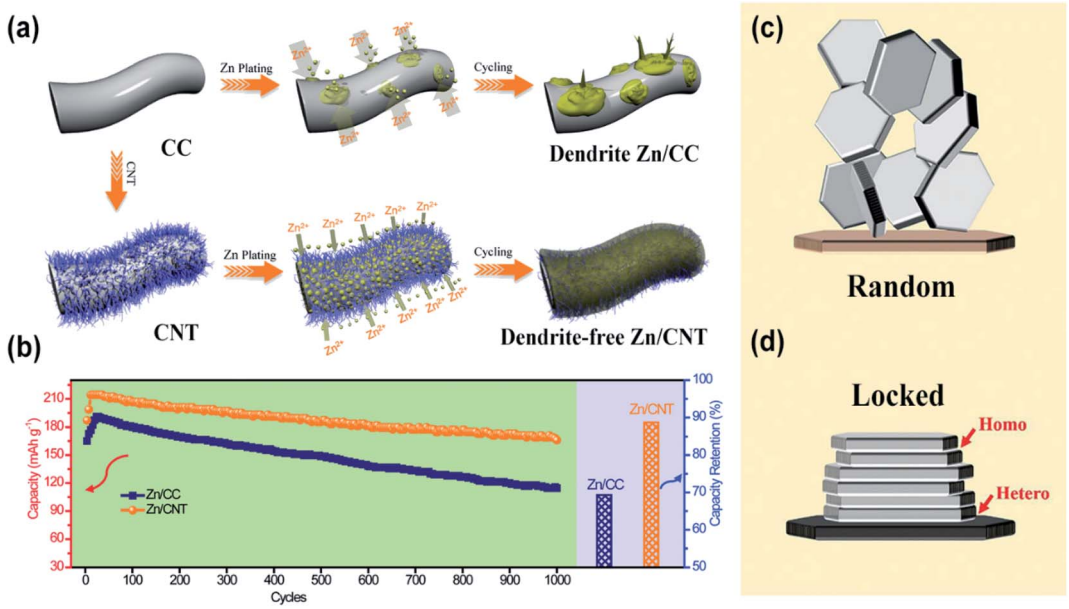

Fig. 7 (a) Schematics of Zn deposition on CC and CNT substrates. (b) Electrochemical performance of the Zn/CC//MnO_2 and Zn/CNT//MnO_2 full cells. Reproduced from ref. 88 with permission. Copyright 2019 Wiley-VCH. Schematic illustrations of (c) intrinsic zinc growth mode and (d) zinc deposition on aligned graphene. Reproduced from ref. 38 with permission. Copyright 2019 The American Association for the Advancement of Science.

Although the high cost is an economic barrier to the widespread application, carbonaceous skeletons loaded with zinc are promising candidates for flexible and wearable electronics because of their excellent mechanical properties and electrochemical performance, which will be further discussed in the next section.

There is also a breakthrough in structural design of substrates to control the zinc crystal growth. Through modifying the basal plane of the graphene substrate, an innovative epitaxial zinc growth strategy is achieved by Archer *et al.*[38] They first revealed the intrinsic growth mode of zinc, in which the exposed close-packed plane (0002) has a lower free energy, leading to a random orientation (Fig. 7c). With the help of aligned graphene, zinc deposits exhibit a smooth zinc layer and locked orientation relationship with the substrate, which can be attributed to the low lattice mismatch between zinc metal and the graphene substrate (Fig. 7d). More surprisingly, this highly ordered deposition pattern is well retained even at a high current density of 40 mA cm^{-2}, indicating the superiority of epitaxial electrodeposition to realize highly reversible metal anodes.

3.1.4 Zinc-free anodes. Zinc-free anodes, which are inspired by rocking-chair lithium ion batteries, are rationally designed to circumvent issues encountered with the zinc metal anode.[89,90] Considering the unstable voltage window of the aqueous electrolytes, there are some vital characteristics zinc-free anodes should have: (1) appropriate zinc insertion potential *versus* Zn/Zn^{2+}, (2) excellent structural stability without obvious dissolution, (3) high initial coulombic efficiency, and (4) highly reversible intercalation/deintercalation dynamics. To date, there is no material completely satisfying all these features. However, the huge progress on zinc-free anodes should not be ignored.

The Chevrel phase ($ZnMo_6S_8$,[91] Mo_6S_8 (ref. 92)) is demonstrated to be a type of potential zinc-free anode. Still, the practical application is technically limited by its poor electrochemical performance. Subsequently, the pre-sodiated TiS_2 with a layered structure is further proposed by Jiang and co-workers.[93] Compared with TiS_2, the developed $Na_{0.14}TiS_2$ not only features improved structural reversibility (Fig. 8a) but also exhibits promoted diffusion kinetics and electrical conductivity. Therefore, it can deliver an initial capacity of 134 mA h g^{-1} with a suitable potential (0.3 V *vs.* Zn/Zn^{2+}) at a high current density of 0.1 A g^{-1} (Fig. 8b) and thus realize an initial capacity of 38 mA h g^{-1} with a capacity retention of more than 70% over 100 cycles for $Na_{0.14}TiS_2||ZnMn_2O_4$ full cells. Recently, hexagonal MoO_3 with a favorable potential of 0.36 V (*vs.* Zn/Zn^{2+}) was reported as a promising zinc intercalation anode.[94] The hexagonal structure endows MoO_3 with fast ion transfer and good structural stability. Consequently, the $MoO_3||Zn_{0.2}MnO_2$ battery exhibits excellent cycling performance after 1000 cycle with a capacity retention of 100%, outperforming the previous reported zinc-free anodes. In addition to above-mentioned materials, mixed-valence $Cu_{2-x}Se$ was proposed by Li *et al.* as a novel interaction-based anode (Fig. 8c).[95] They found that the low valence Cu in $Cu_{2-x}Se$ can not only provide more empty cationic sites but also tune electronic interaction between the active sites and the intercalated Zn^{2+}, resulting in a reduced diffusion barrier and consequently highly reversible reaction (Fig. 8d). With the above merits, the $Cu_{2-x}Se||Zn_xMnO_2$ full cell breaks the previous record of battery lifespan and shows ultralong cycling stability over 20 000 cycles at 2 A g^{-1}, further

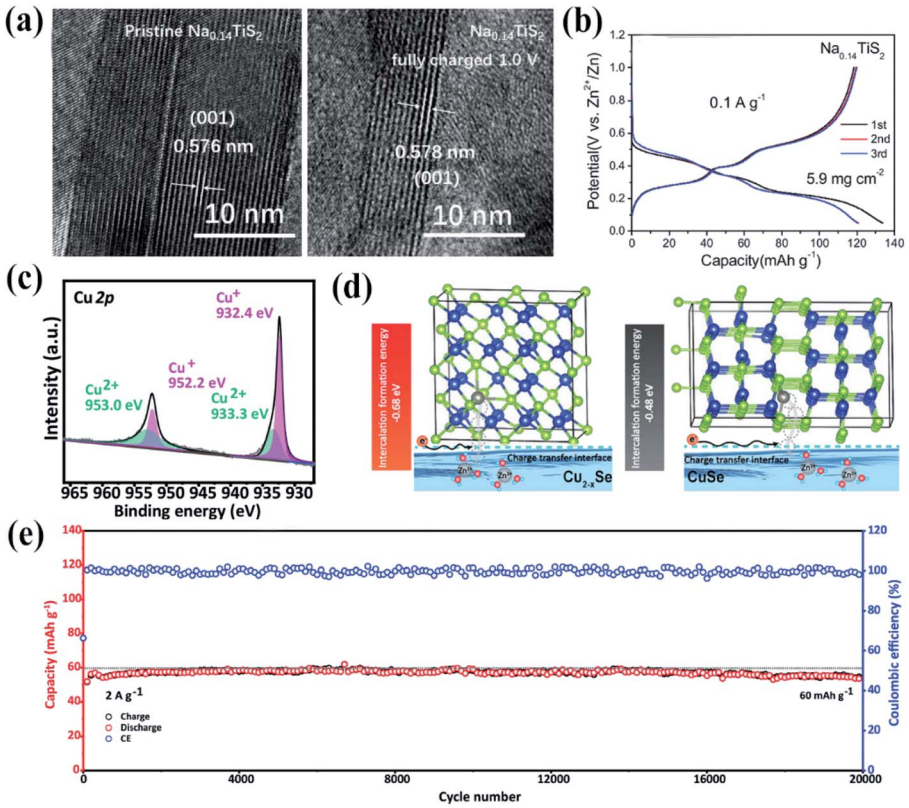

Fig. 8 (a) TEM images of $Na_{0.14}TiS_2$ before and after being charged to 1.0 V, indicating the superior structure stability. (b) The initial three charge/discharge curves of $Na_{0.14}TiS_2$. Reproduced from ref. 93 with permission. Copyright 2019 Wiley-VCH. (c) High-resolution Cu 2p XPS spectra of the $Cu_{2-x}Se$ nanorods. (d) Comparison of the charge transfer process at the reaction interface and intercalation formation energy between $Cu_{2-x}Se$ and CuSe. (e) Long-term cycling performance of $Cu_{2-x}Se$ coupled with Zn_xMnO_2. Reproduced from ref. 95 with permission. Copyright 2019 Wiley-VCH.

improving the application potential of intercalated zinc-free anodes (Fig. 8e).

Nevertheless, despite the effectively improved cycle lifespan and safer working mechanism, the zinc-free anode is still not suitable to be employed for commercialization at present, where high specific capacity and energy density are also needed. Therefore, more potential material candidates are supposed to be explored to realize further breakthroughs.

3.2 Electrolyte strategies

Interface chemistry fundamentally determines the ion transport kinetics and electrochemical behavior of batteries. Hence, in addition to anodes, the electrolyte is also a crucial factor and supposed to be seriously considered. An ideal electrolyte is expected to achieve a reversible Zn plating/stripping process and exhibit a stable electrochemical window within the range of working voltage. Since the emergence of rechargeable ZIBs, most studies are conducted in $ZnSO_4$ aqueous electrolyte. However, AZIBs using the routine electrolyte are inadequate enough to meet the performance requirement, mainly because the zinc metal anode suffers from severe irreversibility issues. In this regard, it is highly desirable to seek another promising electrolyte alternative to solve the problems that have always plagued zinc metal anodes. In this section, we summarize and discuss the optimized aqueous electrolyte system reported to date from two aspects: novel aqueous systems and flexible hydrogel electrolytes.

3.2.1 Novel aqueous system. A concentrated water-in-salt electrolyte (WISE) has been proved to enlarge stable voltage window of aqueous LIBs, and thus greatly reduce hydrogen evolution.[96] Recently Wang *et al.*[27] further explored the possibility of WiSE being applied in rechargeable AZIBs. By rationally designing, a novel WiSE comprising 20 M LiTFSI and 1 M $Zn(TFSI)_2$ was adopted. In this solution, the average number of water molecules available to solvate zinc ion is far below the "solvation numbers" that are well established in conventional electrolytes. Such a unique solvent–ion interaction endows zinc ions with a higher possibility to coordinate with $TFSI^-$ cations rather than forming detrimental hydrated ion complexes, which is confirmed by molecular dynamics (Fig. 9a) and small-angle neutron scattering measurements. Therefore, hydrogen evolution and dendrite formation are effectively alleviated, incurring a highly reversible dendrite-free anode (Fig. 9b) and excellent cycle performance over 4000 cycles (Fig. 9c). Motivated by this work, Ji *et al.*[97] extended the strategy to the $ZnCl_2$ system. A similar mechanism is also applicable to explain the enhanced zinc anode stability and reversibility. However, large-scale application of WiSE is fundamentally restricted by its greatly

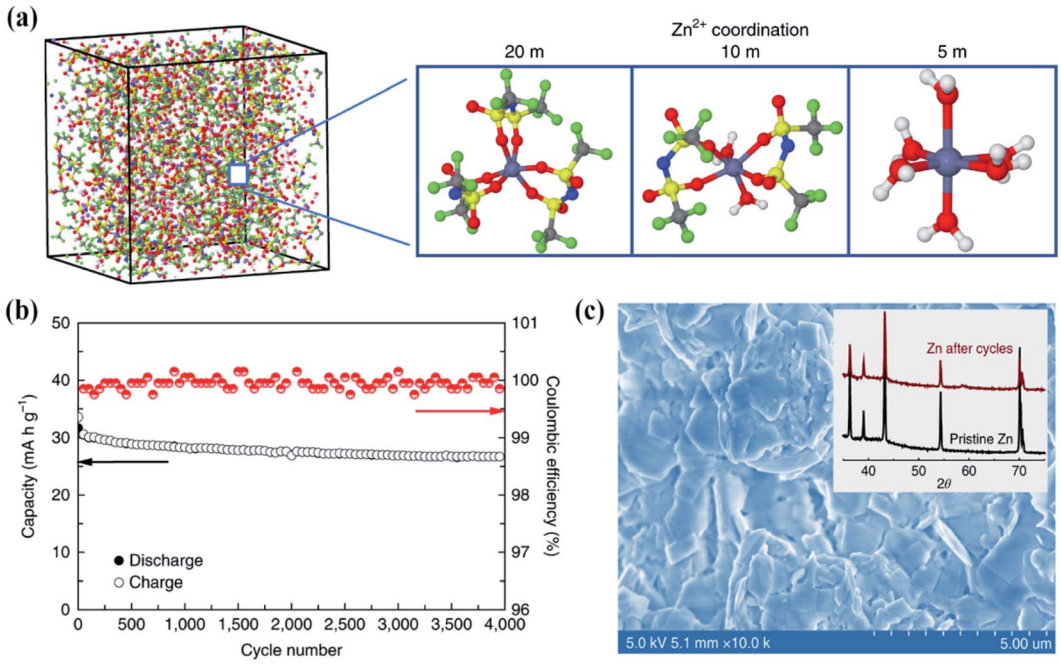

Fig. 9 (a) Molecule dynamics simulation of the solvation sheath in three electrolytes with different concentrations of LiTFSI. (b) Cycling performance of the Zn/$LiMn_2O_4$ full cell with the electrolyte 1 M $Zn(TFSI)_2$ + 20 M LiTFSI. (c) Even zinc plating surface and XRD patterns (inset) after 500 cycles. Reproduced from ref. 27 with permission. Copyright 2018 Nature Publishing Group.

increased weight and price caused by high electrolyte concentration. Therefore, it is necessary to find an effective and economical strategy.

Replacing traditional zinc salts ($ZnSO_4$) with other alternative species can change zinc solvation structures, thereby leading to different interfacial chemistries.[13] To readily capture the zinc ions, electrolytes with low desolvation energy consumption and high ion-transference kinetics are preferred. Through rigorous screening, Chen *et al.*[98] successfully applied $Zn(CF_3SO_3)_2$ salt to aqueous ZIBs. Compared with $ZnSO_4$, $Zn(CF_3SO_3)_2$ features higher water solubility and a wider electrochemical window (2.5 V). More importantly, $Zn(CF_3SO_3)_2$ can modulate the electrolyte structure and decrease the water molecules in the solvation sheath. Consequently, the Zn/electrolyte interface is stabilized and side reactions are mitigated (Fig. 10a), leading to higher coulombic efficiency, lower overpotential, and better cycling performance (Fig. 10b). This inspiring research laid the ground work for our deep understanding of the AZIBs. However, the extremely high cost limits its potential for large-scale energy storage. In addition, the availability of other cheaper alternatives, including $ZnCl_2$,[97] $Zn(CH_3COO)_2$ (ref. 99 and 100) and $Zn(NO_3)_2$,[101] has also been explored. Among them, the $ZnCl_2$ based electrolyte is becoming increasingly popular recently, due to its ultrahigh solubility in water (>30 M) and its tunable electrolyte structure.[102] Chen *et al.*[103] rationally designed a series of low-temperature operating electrolytes by adopting different concentrations of $ZnCl_2$ metal salts (Fig. 10c). After experimental optimization and theoretical simulation, the best concentration is found to be 7.5 M. It is characterized with the lowest solid–liquid transition temperature of −114 °C, high ionic conductivity (1.79 mS cm^{-1} at −60 °C), and excellent compatibility with Zn in the wide range of −100 ∼ +60 °C. The breakage of the original hydrogen-bond network and moderate ion interaction are responsible for this huge improvement (Fig. 10d). With the help of the electrolyte, even at −70 °C, the symmetrical cell achieves reversible Zn plating/stripping (Fig. 10e), and the polyaniline||Zn full batteries exhibit a high capacity of 84.9 mA h g^{-1} with nearly 100% capacity retention over 2000 cycles.

Apart from searching for potential zinc salt alternatives, there is also some progress on electrolyte additives.[104,105] Among them, the metal salt is one of the typical additives. It has been revealed that adding an appropriate amount of $MnSO_4$ into the $ZnSO_4$ electrolyte not only suppresses the dissolution of Mn cations from Mn-based cathodes but also contributes to a stable zinc-electrolyte interface.[106] Such a simple yet effective method offers potential directions for future electrolyte research. Furthermore, the addition of Na_2SO_4 is proved to induce a dendrite-free zinc plating layer (Fig. 11a). During zinc deposition, the Na^+ with a lower reduction potential than Zn^{2+} tends to form a positively charged electrostatic shield layer, driving subsequent zinc ions to the adjacent regions rather than the initial tips of protuberances. At the same time, on the cathode side, the dissolution equilibrium of Na^+ from the $NaV_3O_8 \cdot 1.5H_2O$ (NVO) is broken, altered, and ultimately reformed, resulting in greatly suppressed Na^+ cation dissolution (Fig. 11b).[107] Inspired by this work, our group further systematically investigated the availability of $MgSO_4$ as an additive in the $ZnSO_4$ electrolyte and found the optimized concentration when assembled with the $Mg_xV_2O_5 \cdot nH_2O$ cathode, which is 1 M $ZnSO_4$ + 1 M $MgSO_4$.[108]

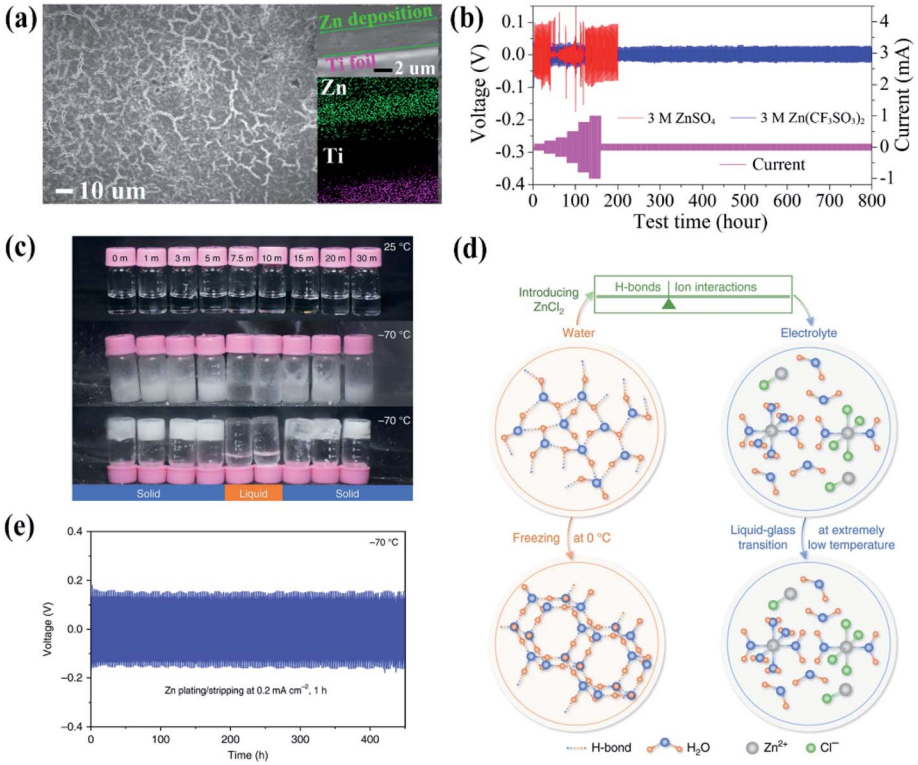

Fig. 10 (a) SEM images and elemental mapping of Zn deposit on Ti foil. (b) Cycling performance of Zn/Zn symmetrical cells in 3 M $ZnSO_4$ and 3 M $Zn(CF_3SO_3)_2$ electrolytes. Reproduced from ref. 98 with permission. Copyright 2016 American Chemical Society. (c) The optical images of different concentration of the $ZnCl_2$ electrolyte at 25 and −70 °C. (d) The schematic illustration of the structure evolutions of water and electrolyte regarding H-bonds and ion interactions. (e) The cycling performance of the Zn symmetric cell at −70 °C. Reproduced from ref. 103 with permission. Copyright 2020 Nature Publishing Group.

In addition, it is acknowledged that some specific polar organic solvents, surfactants, and water-soluble polymers in the electrolyte can also adsorb on the zinc anode surface and manipulate the interfacial electrochemical process. Wang *et al.*[109] reported that a small amount of the diethyl ether (Et_2O) additive is applicable to enhance the cycling performance of AZIBs. When 2 vol% Et_2O is introduced into the aqueous $ZnSO_4$ electrolyte, the polar Et_2O molecules tend to be adsorbed on initial tips of protuberances, which effectively serves as a protecting layer and drives subsequent zinc ion movement to the even surface covered by minimal Et_2O. As a result, the self-amplifying tip effect is fundamentally weakened, thus forming an even zinc plating surface (Fig. 11c). Similarly, a low-cost and nontoxic tetrabutylammonium sulfate (TBA_2SO_4) electrolyte additive strategy was developed by Zhu *et al.*[110] This cationic surfactant enables uniform Zn plating *via* a unique zincophobic repulsion mechanism. With the strong repulsion effect between Zn^{2+} and TBA^+ adsorbed on the Zn surface, the Zn^{2+} cations would be selectively deposited on the flat surface in the vicinity of the tips, leading to a dendrite-free deposition pattern. Furthermore, Qian *et al.*[111] also demonstrated that an optimized concentration of sodium dodecyl sulfate (SDS) adsorbed on the anode surface could expand the electrochemical stability window and restrain severe corrosion as well as Zn dendrites. However, excessive adhesion of additives is inclined to increase interface resistance and polarization, resulting in decreased electrical conductivity of electrodes. For example, a higher concentration of Et_2O is demonstrated to result in a weakened suppression effect. This principle also applies to the cases with a similar mechanism, such as PEG[112] and PAM.[61]

Except for the shielding effect, the introduction of organic solvent additives can also modulate the electrolyte structure to stabilize Zn anodes. For example, ethylene glycol (EG) was employed in aqueous $ZnSO_4$ electrolyte. As the concentration increases, the water molecules in the solvation sheath are gradually substituted by EG. Such a change in the solvation structure not only increases the nucleation overpotential and drives Zn^{2+} to homogeneously diffuse to nucleation sites, but also circumvents the water-related side reactions *via* the formation of abundant H-bonds between water molecules (Fig. 11d).[113] Similarly, amphiphilic 1,2-dimethoxyethane (DME) with unlimited mutual solubility in water holds great potential in constructing H-bonds with H_2O. Recently, Yi *et al.*[114] adopted this tactic and successfully reduced the reactivity of free H_2O (Fig. 11e). The stabilized free water molecules bonded with ether oxygen of DME, fundamentally alleviating corrosion and H_2 evolution.

In short, novel aqueous systems have been developed to improve the electrochemical performance of Zn anodes and full batteries, including ultrahigh concentration WISEs, adoption of new metal salts, and introduction of additives. Among them, some strategies are very effective, but the cost increase cannot

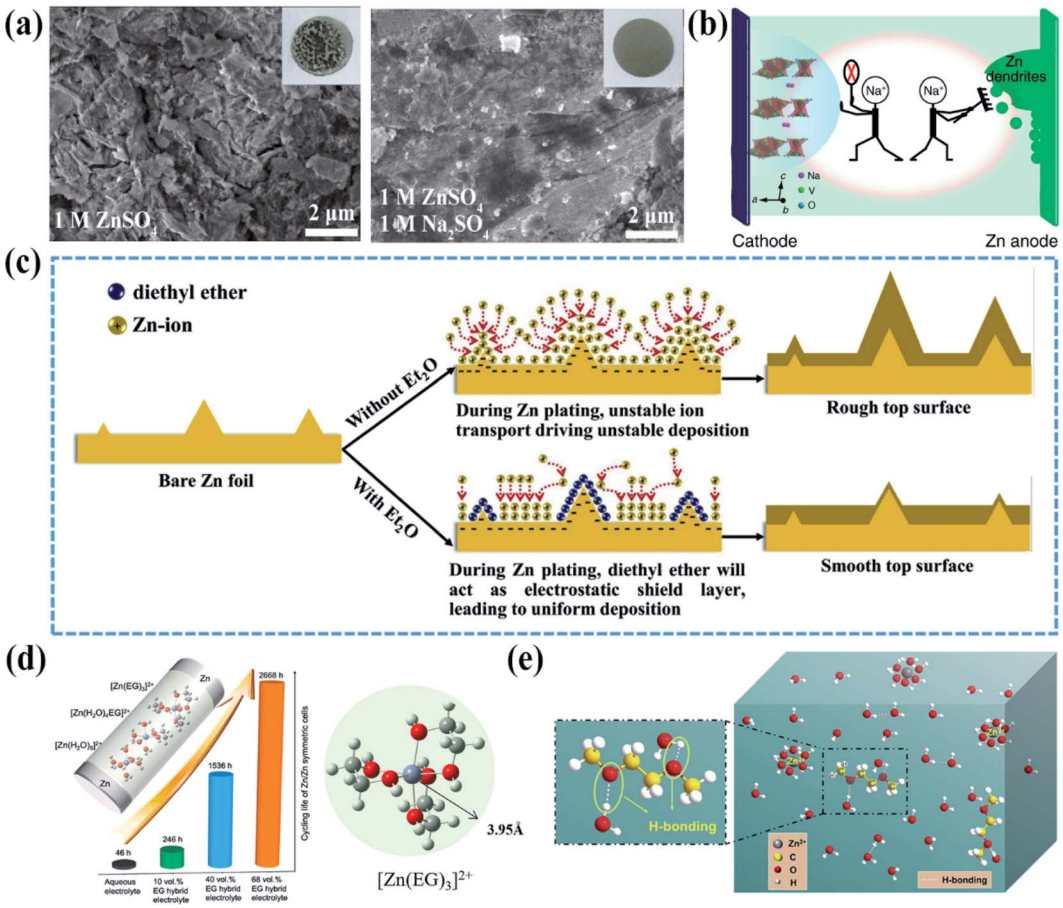

Fig. 11 (a) SEM images of the zinc anode after 500 cycles in 1 M $ZnSO_4$, and 1 M $ZnSO_4$ + 1 M Na_2SO_4 electrolytes. (b) Suppressed dendrite formation and dissolution of NVO nanobelts due to the Na_2SO_4 additive. Reproduced from ref. 107 with permission. Copyright 2018 Nature Publishing Group. (c) Schematic representation of zinc morphology in the electrolyte with and without Et_2O. Reproduced from ref. 109 with permission. Copyright 2019 Elsevier. (d) Schematic representation of the coordination state of Zn^{2+} in H_2O/EG hybrid electrolytes. Reproduced from ref. 113 with permission. Copyright 2020 Elsevier. (e) Schematic illustration of H-bonds in the aqueous electrolyte with a low concentration of DME. Reproduced from ref. 114 with permission. Copyright 2020 Elsevier.

be ignored. In this regard, the additive with the minimum addition amount and environmental benignity is the most optimized solution.

3.2.2 Flexible hydrogel electrolyte. With the increasing requirement for smart wearable electronic devices, the development of flexible rechargeable batteries is urgently needed. Due to its unique features, such as decent ionic conductivity, high security, and excellent mechanical properties, flexible AZIBs have been employed as a potential candidate for flexible and wearable electronic devices.[15,115,116]

Generally, a hydrophilic 3D hydrogel network realized by physical/chemical crosslinking is a key component of flexible ZIBs. It not only serves as an electrolyte to conduct charges between the cathode and anode, but also acts as a separator to provide ionic movement channels.[117,118] Compared with traditional aqueous electrolytes, the hierarchical porous hydrogel with intrinsically fewer free water molecules and a restricted ion diffusion path is superior to tackle the problems of zinc metal.[119] Some inspiring progress has been achieved in the last few years.[84,85,120,121] For example, Zhou *et al.*[122] proposed a new hydrogel-based ZIB, in which the sodium alginate is crosslinked with zinc ions, thus forming mechanically stable zinc alginate gel (Alg–Zn) with fast ion transference. In addition to excellent cycle stability and rate performance, it is also characterized with the merits of satisfactory shelf life and restoration capacity. The superior electrochemical properties are mainly attributed to the mitigated zinc dendrite growth and parasitic reactions induced by ion-guided effects from carboxylate groups (Fig. 12a). Recently, Chen *et al.*[123] developed a borax-crosslinked polyvinyl alcohol (PVA)/glycerol hydrogel electrolyte (denoted as PVA-B-G). In this electrolyte, the polymer chains from the hydrogel provide an electrostatic shield for zinc anodes and water molecules are strongly constrained by glycerol. As a result, a dendrite-free surface (Fig. 12b) and eliminated by-products (Fig. 12c) are realized for the zinc anode, and thus, the PVA-B-G batteries are capable of retaining 90% capacity after 2000 cycles.

The electrolytes with unique properties have also been intensively studied.[118] Chen *et al.*[124] successfully incorporated zinc ionic species into the PVA matrix and developed a special

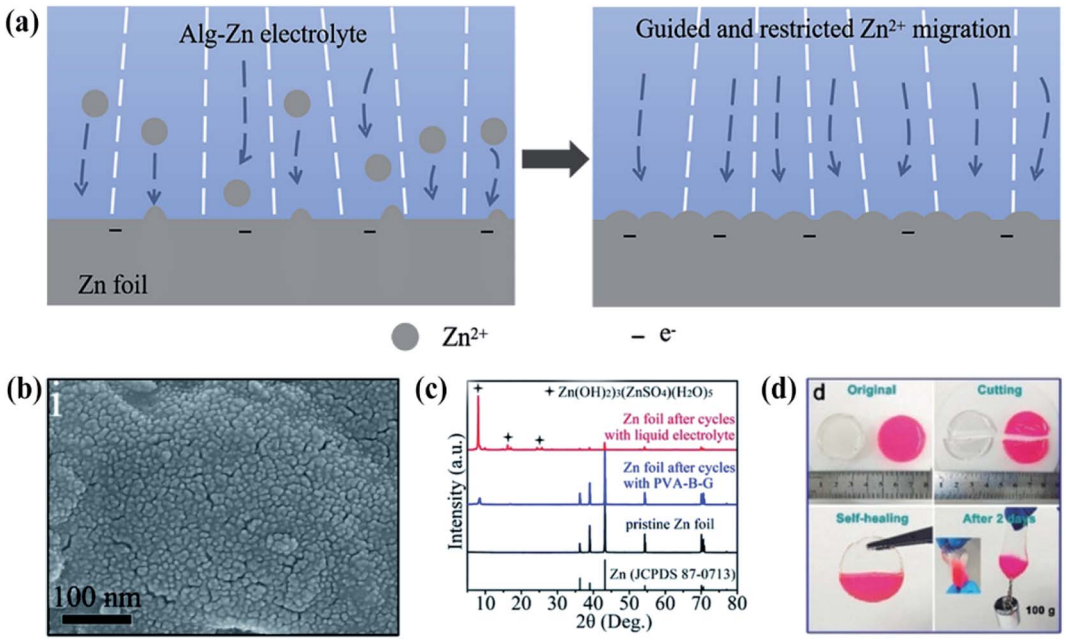

Fig. 12 (a) The mechanism of zinc deposition behavior in the Alg–Zn electrolyte. Reproduced from ref. 122 with permission. Copyright 2020 Elsevier. (b) Dendrite-free surface of zinc metal with PVA-B-G. (c) XRD patterns of bare zinc and zinc foil cycling for 2000 cycles. Reproduced from ref. 123 with permission. Copyright 2020 The Royal Society of Chemistry. (d) Illustration of self-healing capability of the PVA-based hydrogel electrolyte. Reproduced from ref. 124 with permission. Copyright 2019 Wiley-VCH.

self-healing PVA/Zn$(CF_3SO_3)_2$ hydrogel electrolyte (Fig. 12d). Even after several times of cutting, the fracture surface can be healed and the electrochemical performance is completely recovered. Furthermore, many other kinds of functional hydrogel electrolytes have been rationally designed, such as anti-freezing electrolytes,[125,126] smartly self-protective electrolytes[127] and intelligently cooling-recovery electrolytes,[128] all of which ensure a smooth migration of zinc ions and reversible cycling of zinc anodes.

4 Summary and future perspectives

As a new-generation sustainable energy storage system, AZIBs have been developing rapidly in recent years since the zinc metal anode exhibits a unique combination of high theoretical capacity and natural abundance. However, the dendrite growth and parasitic side reactions plaguing zinc metal anodes need to be addressed to realize practical applications of AZIBs. In this review, we first analyzed thermodynamic origins and fundamentals of the above problems. Then, we elaborated tactics regarding interface regulation of the Zn anode, which spans from anodic studies to electrolyte design. Despite recent advances in realizing a high-performance Zn anode, there are still some perplexing problems to be further explored. Hence, some outlooks and future development direction are accordingly proposed as follows:

(1) Currently, almost all studies of AZIBs are focusing on the performance of coin cells rather than commercial products. There is still a huge gap between laboratory-based research studies and practical application. Although some metrics, such as DOD, charging/discharging current density, and areal capacity, are very important under practical conditions, they are generally ignored in the laboratory. For example, electronics with fast cycling rate and specific energy density have been always pursued by the consumer market. This means that high current density and efficient utility of the Zn anode should be realized in batteries. However, these requirements would inevitably degrade the electrochemical performance due to more severe anodic problems. Therefore, it is recommended to provide these valuable metrics to help promote continuous progress in Zn anodes and AZIBs.

(2) Zn alloying is the most promising method for large-scale preparation. It is generally accepted that the electrochemical properties of alloys are determined from chemical compositions and phase constitutions. Up to now, a few zinc alloy anodes are investigated for AZIBs. Looking ahead, more alloy systems with diversified composition are supposed to be considered. *Via* thermodynamic phase diagrams coupled with reported experimental results, useful alloying parameters and phase information can be obtained. These results enable us to effectively predict and design some special architectures, such as uniformly dispersed nanophases in the zinc matrix. The obtained unique phase distribution is expected to fundamentally improve the zinc diffusion mode and realize the dendrite-free zinc plating surface.

(3) In consideration of the complex interrelation between problems facing the zinc anode in aqueous media, it is very challenging to employ comprehensively effective approaches to tackle them simultaneously. Intrinsic properties of the hydrogel electrolyte enable zinc ions to form a homogeneous flux and

limit the number of free water molecules to reduce the possibility of interfacial side reactions. Therefore, it is a feasible proposal to develop eco-friendly and cost-effective hydrogels that can be adopted for practical use. However, completely eliminating the detrimental dendrite growth is hard to realize. In this regard, functional electrolytes with exceptional mechanical properties and anti-puncturing capability are worth further exploring. Furthermore, a non-aqueous gel polymer with the function of a separator and electrolyte may be an ideal solution without considering the increased cost.

(4) From a fundamental point of view, it is urgently needed to accelerate the exploration of zinc-electrolyte interfacial chemistry. The current investigation of solvation structures is mainly based on *ex situ* analysis and theoretical simulation, which is not comprehensive enough to deeply understand chemical changes at the anode/electrolyte interface. Thanks to the ever-developing technology, advanced *in situ* characterization is constantly emerging, by which the atomic interaction between active species and solvent media, and accurate element and valance analysis of solvation-sheath during the dynamic solvation/desolvation process can be possibly probed in the future.

(5) In present, most studies regarding zinc dendrite issues mainly refer to already established fundamentals of alkali metals in organic electrolytes. However, for AZIBs, both the water-based environment and the flake-like morphology of zinc deposits are different. Therefore, it is recommended to construct an exclusive nucleation and growth theory. Moreover, the electrochemical performance of metallic materials is relevant to grain orientation. To realize a fixed growth orientation and dendrite-free anode surface, efforts are suggested to be focused on the texture evolution and regulation for the zinc metal anode, which could be readily realized by plastic deformation process and dynamic crystallization.

Conflicts of interest

The authors declare no conflict of interest.

Acknowledgements

This work is supported by the Singapore Ministry of Education academic research grant Tier 2 (MOE2019-T2-1-181).

References

1 Y. Shang, X. Li, S. Huang, S. Chen, Z. Yang, L. Guo and H. Y. Yang, *Matter*, 2020, **2**, 428–439.
2 Y. Shang, X. X. Li, J. J. Song, S. Z. Huang, Z. Yang, Z. C. J. Xu and H. Y. Yang, *Chem*, 2020, **6**, 1804–1818.
3 R. W. Mo, D. Rooney, K. N. Sun and H. Y. Yang, *Nat. Commun.*, 2017, **8**, 13949.
4 Y. M. Shi, Y. Wang, J. I. Wong, A. Y. S. Tan, C. L. Hsu, L. J. Li, Y. C. Lu and H. Y. Yang, *Sci. Rep.*, 2013, **3**, 2169.
5 L. G. Lu, X. B. Han, J. Q. Li, J. F. Hua and M. G. Ouyang, *J. Power Sources*, 2013, **226**, 272–288.
6 T. Famprikis, P. Canepa, J. A. Dawson, M. S. Islam and C. Masquelier, *Nat. Mater.*, 2019, **18**, 1278–1291.
7 G. Z. Li, B. Huang, Z. F. Pan, X. Y. Su, Z. P. Shao and L. An, *Energy Environ. Sci.*, 2019, **12**, 2030–2053.
8 X. Wu, Y. L. Chen, Z. Xing, C. W. K. Lam, S. S. Pang, W. Zhang and Z. C. Ju, *Adv. Energy Mater.*, 2019, **9**, 1900343.
9 S. Chen, S. Z. Huang, J. P. Hu, S. Fan, Y. Shang, M. E. Pam, X. X. Li, Y. Wang, T. L. Xu, Y. M. Shi and H. Y. Yang, *Nano-Micro Lett.*, 2019, **11**, 80.
10 X. L. Li, T. C. Li, S. Z. Huang, J. Zhang, M. E. Pam and H. Y. Yang, *ChemSusChem*, 2020, **13**, 1379–1391.
11 Z. X. Liu, Y. Huang, Y. Huang, Q. Yang, X. L. Li, Z. D. Huang and C. Y. Zhi, *Chem. Soc. Rev.*, 2020, **49**, 180–232.
12 R. Schmuch, R. Wagner, G. Hörpel, T. Placke and M. Winter, *Nat. Energy*, 2018, **3**, 267–278.
13 B. Tang, L. Shan, S. Liang and J. Zhou, *Energy Environ. Sci.*, 2019, **12**, 3288–3304.
14 T.-H. Wu, Y. Zhang, Z. D. Althouse and N. Liu, *Mater. Today Nano*, 2019, **6**, 100032.
15 H. F. Li, L. T. Ma, C. P. Han, Z. F. Wang, Z. X. Liu, Z. J. Tang and C. Y. Zhi, *Nano Energy*, 2019, **62**, 550–587.
16 F. Liu, Z. X. Chen, G. Z. Fang, Z. Q. Wang, Y. S. Cai, B. Y. Tang, J. Zhou and S. Q. Liang, *Nano-Micro Lett.*, 2019, **11**, 25.
17 N. Zhang, M. Jia, Y. Dong, Y. Y. Wang, J. Z. Xu, Y. C. Liu, L. F. Jiao and F. Y. Cheng, *Adv. Funct. Mater.*, 2019, **29**, 1807331.
18 C. Y. Zhu, G. Z. Fang, J. Zhou, J. H. Guo, Z. Q. Wang, C. Wang, J. Y. Li, Y. Tang and S. Q. Liang, *J. Mater. Chem. A*, 2018, **6**, 9677–9683.
19 L. T. Ma, S. M. Chen, C. B. Long, X. L. Li, Y. W. Zhao, Z. X. Liu, Z. D. Huang, B. B. Dong, J. A. Zapien and C. Y. Zhi, *Adv. Energy Mater.*, 2019, **9**, 1902446.
20 C. Li, X. Xie, S. Liang and J. Zhou, *Energy Environ. Mater.*, 2020, **3**, 146–159.
21 G. Fang, J. Zhou, A. Pan and S. Liang, *ACS Energy Lett.*, 2018, **3**, 2480–2501.
22 Z. Q. Zhao, X. Y. Fan, J. Ding, W. B. Hu, C. Zhong and J. Lu, *ACS Energy Lett.*, 2019, **4**, 2259–2270.
23 X. Xie, S. Liang, J. Gao, S. Guo, J. Guo, C. Wang, G. Xu, X. Wu, G. Chen and J. Zhou, *Energy Environ. Sci.*, 2020, **13**, 503–510.
24 Z. Cai, Y. T. Ou, J. D. Wang, R. Xiao, L. Fu, Z. Yuan, R. M. Zhan and Y. M. Sun, *Energy Storage Mater.*, 2020, **27**, 205–211.
25 D. L. Han, S. C. Wu, S. W. Zhang, Y. Q. Deng, C. J. Cui, L. A. Zhang, Y. Long, H. Li, Y. Tao, Z. Weng, Q. H. Yang and F. Y. Kang, *Small*, 2020, **16**, 2001736.
26 J. N. Hao, X. L. Li, S. L. Zhang, F. H. Yang, X. H. Zeng, S. Zhang, G. Y. Bo, C. S. Wang and Z. P. Guo, *Adv. Funct. Mater.*, 2020, **30**, 2001263.
27 F. Wang, O. Borodin, T. Gao, X. Fan, W. Sun, F. Han, A. Faraone, J. A. Dura, K. Xu and C. Wang, *Nat. Mater.*, 2018, **17**, 543–549.
28 Q. Yang, G. Liang, Y. Guo, Z. Liu, B. Yan, D. Wang, Z. Huang, X. Li, J. Fan and C. Zhi, *Adv. Mater.*, 2019, **31**, 1903778.

29 Y. Xu, T. Li, L. Wang and Y. Kang, *Adv. Mater.*, 2019, **31**, 1901662.
30 H. Li, D. Chao, B. Chen, X. Chen, C. Chuah, Y. Tang, Y. Jiao, M. Jaroniec and S.-Z. Qiao, *J. Am. Chem. Soc.*, 2020, **142**, 2012–2022.
31 S. K. Heiskanen, J. Kim and B. L. Lucht, *Joule*, 2019, **3**, 2322–2333.
32 M. Li, J. Lu, X. L. Ji, Y. G. Li, Y. Y. Shao, Z. W. Chen, C. Zhong and K. Amine, *Nat. Rev. Mater.*, 2020, **5**, 276–294.
33 A. Hagopian, M.-L. Doublet and J.-S. Filhol, *Energy Environ. Sci.*, 2020, **13**, 5186–5197.
34 A. K. Lautar, D. Kopac, T. Rejec, T. Bancic and R. Dominko, *Phys. Chem. Chem. Phys.*, 2019, **21**, 2434–2442.
35 C. Han, W. Li, H. K. Liu, S. Dou and J. Wang, *Nano Energy*, 2020, **74**, 104880.
36 W. Lu, C. Xie, H. Zhang and X. Li, *ChemSusChem*, 2018, **11**, 3996–4006.
37 J. Zheng, J. Yin, D. Zhang, G. Li, D. C. Bock, T. Tang, Q. Zhao, X. Liu, A. Warren and Y. Deng, *Sci. Adv.*, 2020, **6**, eabb1122.
38 J. Zheng, Q. Zhao, T. Tang, J. Yin, C. D. Quilty, G. D. Renderos, X. Liu, Y. Deng, L. Wang, D. C. Bock, C. Jaye, D. Zhang, E. S. Takeuchi, K. J. Takeuchi, A. C. Marschilok and L. A. Archer, *Science*, 2019, **366**, 645–649.
39 Q. Yang, Y. Guo, B. Yan, C. Wang, Z. Liu, Z. Huang, Y. Wang, Y. Li, H. Li and L. Song, *Adv. Mater.*, 2020, **32**, 2001755.
40 B. Beverskog and I. Puigdomenech, *Corros. Sci.*, 1997, **39**, 107–114.
41 J. N. Hao, X. L. Li, X. H. Zeng, D. Li, J. F. Mao and Z. P. Guo, *Energy Environ. Sci.*, 2020, **13**, 3917–3949.
42 A. P. Murthy, J. Theerthagiri and J. Madhavan, *J. Phys. Chem. C*, 2018, **122**, 23943–23949.
43 E. Gileadi and E. Kirowa-Eisner, *Corros. Sci.*, 2005, **47**, 3068–3085.
44 J. N. Hao, B. Li, X. L. Li, X. H. Zeng, S. L. Zhang, F. H. Yang, S. L. Liu, D. Li, C. Wu and Z. P. Guo, *Adv. Mater.*, 2020, **32**, 2003021.
45 H. Qiu, X. Du, J. Zhao, Y. Wang, J. Ju, Z. Chen, Z. Hu, D. Yan, X. Zhou and G. Cui, *Nat. Commun.*, 2019, **10**, 5374.
46 J. Fu, Z. P. Cano, M. G. Park, A. Yu, M. Fowler and Z. Chen, *Adv. Mater.*, 2017, **29**, 1604685.
47 Z. Li, K. G. Pradeep, Y. Deng, D. Raabe and C. C. Tasan, *Nature*, 2016, **534**, 227–230.
48 Y. Lu, Y. Dong, S. Guo, L. Jiang, H. Kang, T. Wang, B. Wen, Z. Wang, J. Jie and Z. Cao, *Sci. Rep.*, 2014, **4**, 6200.
49 O. Senkov, G. Wilks, D. Miracle, C. Chuang and P. Liaw, *Intermetallics*, 2010, **18**, 1758–1765.
50 B. Schuh, F. Mendez-Martin, B. Volker, E. P. George, H. Clemens, R. Pippan and A. Hohenwarter, *Acta Mater.*, 2015, **96**, 258–268.
51 J. Frenzel, Z. Zhang, K. Neuking and G. Eggeler, *J. Alloys Compd.*, 2004, **385**, 214–223.
52 W. Guo, B. Liu, Y. Liu, T. Li, A. Fu, Q. Fang and Y. Nie, *J. Alloys Compd.*, 2019, **776**, 428–436.
53 T. C. Li, B. Liu, Y. Liu, W. M. Guo, A. Fu, L. S. Li, N. Yan and Q. H. Fang, *Entropy*, 2018, **20**, 517.
54 T. C. Li, Y. Liu, B. Liu, W. M. Guo and L. Y. Xu, *Coatings*, 2017, **7**, 151.
55 Y. Peng, W. Zhang, T. Li, M. Zhang, B. Liu, Y. Liu, L. Wang and S. Hu, *Surf. Coat. Technol.*, 2020, **385**, 125326.
56 Y. B. Peng, W. Zhang, T. C. Li, M. Y. Zhang, L. Wang, Y. Song, S. H. Hu and Y. Hu, *Int. J. Refract. Met. Hard Mater.*, 2019, **84**, 105044.
57 X. Liang, Q. Pang, I. R. Kochetkov, M. S. Sempere, H. Huang, X. Sun and L. F. Nazar, *Nat. Energy*, 2017, **2**, 17119.
58 S.-B. Wang, Q. Ran, R.-Q. Yao, H. Shi, Z. Wen, M. Zhao, X.-Y. Lang and Q. Jiang, *Nat. Commun.*, 2020, **11**, 1–9.
59 Z. Jia, T. Yang, L. Sun, Y. Zhao, W. Li, J. Luan, F. Lyu, L. C. Zhang, J. J. Kruzic and J. J. Kai, *Adv. Mater.*, 2020, **32**, 2000385.
60 X. Gao, Y. Lu, B. Zhang, N. Liang, G. Wu, G. Sha, J. Liu and Y. Zhao, *Acta Mater.*, 2017, **141**, 59–66.
61 Q. Zhang, J. Luan, L. Fu, S. Wu, Y. Tang, X. Ji and H. Wang, *Angew. Chem., Int. Ed.*, 2019, **58**, 15841–15847.
62 M. S. Azevedo, C. Allely, K. Ogle and P. Volovitch, *Corros. Sci.*, 2015, **90**, 482–490.
63 S. Das, S. Jena, S. Banthia, A. Mitra, S. Das and K. Das, *J. Alloys Compd.*, 2019, **792**, 770–779.
64 H. Jia, Z. Wang, B. Tawiah, Y. Wang, C.-Y. Chan, B. Fei and F. Pan, *Nano Energy*, 2020, **70**, 104523.
65 C. F. Li, S. H. Liu, C. G. Shi, G. H. Liang, Z. T. Lu, R. W. Fu and D. C. Wu, *Nat. Commun.*, 2019, **10**, 1363.
66 Z. Zhao, J. Zhao, Z. Hu, J. Li, J. Li, Y. Zhang, C. Wang and G. Cui, *Energy Environ. Sci.*, 2019, **12**, 1938–1949.
67 C. Deng, X. Xie, J. Han, Y. Tang, J. Gao, C. Liu, X. Shi, J. Zhou and S. Liang, *Adv. Funct. Mater.*, 2020, **30**, 2000599.
68 P. Liang, J. Yi, X. Liu, K. Wu, Z. Wang, J. Cui, Y. Liu, Y. Wang, Y. Xia and J. Zhang, *Adv. Funct. Mater.*, 2020, **30**, 1908528.
69 L. Kang, M. Cui, F. Jiang, Y. Gao, H. Luo, J. Liu, W. Liang and C. Zhi, *Adv. Energy Mater.*, 2018, **8**, 1801090.
70 Y. Li, F. Liang, H. Bux, W. Yang and J. Caro, *J. Membr. Sci.*, 2010, **354**, 48–54.
71 H. Yang, Z. Chang, Y. Qiao, H. Deng, X. Mu, P. He and H. Zhou, *Angew. Chem., Int. Ed.*, 2020, **59**, 9377–9381.
72 Z. Zhou, Y. Zhang, P. Chen, Y. Wu, H. Yang, H. Ding, Y. Zhang, Z. Wang, X. Du and N. Liu, *Chem. Eng. Sci.*, 2019, **194**, 142–147.
73 C. Shen, X. Li, N. Li, K. Xie, J. G. Wang, X. Liu and B. Wei, *ACS Appl. Mater. Interfaces*, 2018, **10**, 25446–25453.
74 A. Xia, X. Pu, Y. Tao, H. Liu and Y. Wang, *Appl. Surf. Sci.*, 2019, **481**, 852–859.
75 L. Dong, W. Yang, W. Yang, H. Tian, Y. Huang, X. Wang, C. Xu, C. Wang, F. Kang and G. Wang, *Chem. Eng. J.*, 2020, **384**, 123355.
76 R. Yuksel, O. Buyukcakir, W. K. Seong and R. S. Ruoff, *Adv. Energy Mater.*, 2020, **10**, 1904215.
77 Z. W. Li, L. Y. Wu, S. Y. Dong, T. Z. Xu, S. P. Li, Y. F. An, J. M. Jiang and X. G. Zhang, *Adv. Funct. Mater.*, 2021, **31**, 2006495.
78 J. F. Parker, C. N. Chervin, I. R. Pala, M. Machler, M. F. Burz, J. W. Long and D. R. Rolison, *Science*, 2017, **356**, 415–418.

79 C. C. Wang, G. Y. Zhu, P. Liu and Q. Chen, *ACS Nano*, 2020, **14**, 2404–2411.
80 D. Lin, Y. Liu, Z. Liang, H.-W. Lee, J. Sun, H. Wang, K. Yan, J. Xie and Y. Cui, *Nat. Nanotechnol.*, 2016, **11**, 626–632.
81 W. Zhang, H. L. Zhuang, L. Fan, L. Gao and Y. Lu, *Sci. Adv.*, 2018, **4**, eaar4410.
82 C. Li, X. Shi, S. Liang, X. Ma, M. Han, X. Wu and J. Zhou, *Chem. Eng. J.*, 2020, **379**, 122248.
83 X. Shi, G. Xu, S. Liang, C. Li, S. Guo, X. Xie, X. Ma and J. Zhou, *ACS Sustainable Chem. Eng.*, 2019, **7**, 17737–17746.
84 H. Li, C. Han, Y. Huang, Y. Huang, M. Zhu, Z. Pei, Q. Xue, Z. Wang, Z. Liu, Z. Tang, Y. Wang, F. Kang, B. Li and C. Zhi, *Energy Environ. Sci.*, 2018, **11**, 941–951.
85 Y. Zeng, X. Zhang, Y. Meng, M. Yu, J. Yi, Y. Wu, X. Lu and Y. Tong, *Adv. Mater.*, 2017, **29**, 1700274.
86 D. Chao, C. Zhu, M. Song, P. Liang, X. Zhang, N. H. Tiep, H. Zhao, J. Wang, R. Wang and H. Zhang, *Adv. Mater.*, 2018, **30**, 1803181.
87 Z. Wang, J. Huang, Z. Guo, X. Dong, Y. Liu, Y. Wang and Y. Xia, *Joule*, 2019, **3**, 1289–1300.
88 Y. Zeng, X. Zhang, R. Qin, X. Liu, P. Fang, D. Zheng, Y. Tong and X. Lu, *Adv. Mater.*, 2019, **31**, 1903675.
89 B. Scrosati, *Electrochim. Acta*, 2000, **45**, 2461–2466.
90 X. L. Li, T. C. Li, S. Huang, J. Zhang, M. E. Pam and H. Y. Yang, *ChemSusChem*, 2020, **13**, 1379–1391.
91 M. S. Chae, J. W. Heo, S.-C. Lim and S.-T. Hong, *Inorg. Chem.*, 2016, **55**, 3294–3301.
92 Y. Cheng, L. Luo, L. Zhong, J. Chen, B. Li, W. Wang, S. X. Mao, C. Wang, V. L. Sprenkle and G. Li, *ACS Appl. Mater. Interfaces*, 2016, **8**, 13673–13677.
93 W. Li, K. L. Wang, S. J. Cheng and K. Jiang, *Adv. Energy Mater.*, 2019, **9**, 1900993.
94 T. Xiong, Y. Zhang, Y. Wang, W. S. V. Lee and J. Xue, *J. Mater. Chem. A*, 2020, **8**, 9006–9012.
95 Y. Yang, J. F. Xiao, J. Y. Cai, G. M. Wang, W. C. Du, Y. F. Zhang, X. H. Lu and C. C. Li, *Adv. Funct. Mater.*, 2021, **31**, 2005092.
96 L. Suo, O. Borodin, T. Gao, M. Olguin, J. Ho, X. Fan, C. Luo, C. Wang and K. Xu, *Science*, 2015, **350**, 938–943.
97 C. Zhang, J. Holoubek, X. Wu, A. Daniyar, L. Zhu, C. Chen, D. P. Leonard, I. A. Rodríguez-Pérez, J.-X. Jiang and C. Fang, *Chem. Commun.*, 2018, **54**, 14097–14099.
98 N. Zhang, F. Cheng, Y. Liu, Q. Zhao, K. Lei, C. Chen, X. Liu and J. Chen, *J. Am. Chem. Soc.*, 2016, **138**, 12894–12901.
99 G. Li, Z. Yang, Y. Jiang, C. Jin, W. Huang, X. Ding and Y. Huang, *Nano Energy*, 2016, **25**, 211–217.
100 B. Zhang, Y. Liu, X. Wu, Y. Yang, Z. Chang, Z. Wen and Y. Wu, *Chem. Commun.*, 2014, **50**, 1209–1211.
101 J. Zhou, L. T. Shan, Z. X. Wu, X. Guo, G. Z. Fang and S. Q. Liang, *Chem. Commun.*, 2018, **54**, 4457–4460.
102 T. Zhang, Y. Tang, S. Guo, X. Cao, A. Pan, G. Fang, J. Zhou and S. Liang, *Energy Environ. Sci.*, 2020, **13**, 4625–4665.
103 Q. Zhang, Y. Ma, Y. Lu, L. Li, F. Wan, K. Zhang and J. Chen, *Nat. Commun.*, 2020, **11**, 4463.
104 Y. Zhang, Z. Chen, H. Qiu, W. Yang, Z. Zhao, J. Zhao and G. Cui, *NPG Asia Mater.*, 2020, **12**, 4.
105 S. Guo, L. Qin, T. Zhang, M. Zhou, J. Zhou, G. Fang and S. Liang, *Energy Storage Mater.*, 2021, **34**, 545–562.
106 H. Pan, Y. Shao, P. Yan, Y. Cheng, K. S. Han, Z. Nie, C. Wang, J. Yang, X. Li and P. Bhattacharya, *Nat. Energy*, 2016, **1**, 16039.
107 F. Wan, L. Zhang, X. Dai, X. Wang, Z. Niu and J. Chen, *Nat. Commun.*, 2018, **9**, 1656.
108 Y. M. Zhang, H. N. Li, S. Z. Huang, S. Fan, L. N. Sun, B. B. Tian, F. M. Chen, Y. Wang, Y. M. Shi and H. Y. Yang, *Nano-Micro Lett.*, 2020, **12**, 16.
109 W. Xu, K. Zhao, W. Huo, Y. Wang, G. Yao, X. Gu, H. Cheng, L. Mai, C. Hu and X. Wang, *Nano Energy*, 2019, **62**, 275–281.
110 A. Bayaguud, X. Luo, Y. P. Fu and C. B. Zhu, *ACS Energy Lett.*, 2020, **5**, 3012–3020.
111 Z. Hou, X. Zhang, X. Li, Y. Zhu, J. Liang and Y. Qian, *J. Mater. Chem. A*, 2017, **5**, 730–738.
112 A. Mitha, A. Z. Yazdi, M. Ahmed and P. Chen, *ChemElectroChem*, 2018, **5**, 2409–2418.
113 R. Qin, Y. Wang, M. Zhang, Y. Wang, S. Ding, A. Song, H. Yi, L. Yang, Y. Song and Y. Cui, *Nano Energy*, 2020, **80**, 105478.
114 J. Cui, X. Liu, Y. Xie, K. Wu, Y. Wang, Y. Liu, J. Zhang, J. Yi and Y. Xia, *Mater. Today Energy*, 2020, **18**, 100563.
115 L. E. Blanc, D. Kundu and L. F. Nazar, *Joule*, 2020, **4**, 771–799.
116 W. W. Xu and Y. Wang, *Nano-Micro Lett.*, 2019, **11**, 1802605.
117 P. Yu, Y. X. Zeng, H. Z. Zhang, M. H. Yu, Y. X. Tong and X. Lu, *Small*, 2019, **15**, 1804760.
118 Y. B. Li, J. Fu, C. Zhong, T. P. Wu, Z. W. Chen, W. B. Hu, K. Amine and J. Lu, *Adv. Energy Mater.*, 2019, **9**, 1802605.
119 X. J. Li, Y. C. Tang, H. M. Lv, W. L. Wang, F. N. Mo, G. J. Liang, C. Y. Zhi and H. F. Li, *Nanoscale*, 2019, **11**, 17992–18008.
120 H. Li, Z. Liu, G. Liang, Y. Huang, Y. Huang, M. Zhu, Z. Pei, Q. Xue, Z. Tang, Y. Wang, B. Li and C. Zhi, *ACS Nano*, 2018, **12**, 3140–3148.
121 Z. Liu, D. Wang, Z. Tang, G. Liang, Q. Yang, H. Li, L. Ma, F. Mo and C. Zhi, *Energy Storage Mater.*, 2019, **23**, 636–645.
122 Y. Tang, C. Liu, H. Zhu, X. Xie, J. Gao, C. Deng, M. Han, S. Liang and J. Zhou, *Energy Storage Mater.*, 2020, **27**, 109–116.
123 M. Chen, W. Zhou, A. Wang, A. Huang, J. Chen, J. Xu and C.-P. Wong, *J. Mater. Chem. A*, 2020, **8**, 6828–6841.
124 S. Huang, F. Wan, S. Bi, J. Zhu, Z. Niu and J. Chen, *Angew. Chem., Int. Ed.*, 2019, **131**, 4357–4361.
125 M. Zhu, X. Wang, H. Tang, J. Wang, Q. Hao, L. Liu, Y. Li, K. Zhang and O. G. Schmidt, *Adv. Funct. Mater.*, 2019, **30**, 1907218.
126 F. Mo, G. Liang, Q. Meng, Z. Liu, H. Li, J. Fan and C. Zhi, *Energy Environ. Sci.*, 2019, **12**, 706–715.
127 F. Mo, H. Li, Z. Pei, G. Liang, L. Ma, Q. Yang, D. Wang, Y. Huang and C. Zhi, *Sci. Bull.*, 2018, **63**, 1077–1086.
128 J. Zhao, K. K. Sonigara, J. Li, J. Zhang, B. Chen, J. Zhang, S. S. Soni, X. Zhou, G. Cui and L. Chen, *Angew. Chem., Int. Ed.*, 2017, **129**, 7979–7983.

